Supplement of Atmos. Chem. Phys., 19, 1147–1172, 2019
https://doi.org/10.5194/acp-19-1147-2019-supplement

Supplement of

Cloud feedbacks in extratropical cyclones: insight from long-term satellite data and high-resolution global simulations

Daniel T. McCoy et al.

Correspondence to: Daniel T. McCoy (d.t.mccoy@leeds.ac.uk)

1. Description of models used in the main text

In this section we give an expanded discussion of specific models listed in Table 2.

1.1 EC-Earth

The EC-Earth model used for HighResMIP/PRIMAVERA is part of the EC-Earth3-familiy. EC-Earth 3 is a successor of the version 2.3 used for CMIP5 (Hazeleger et al., 2012). The version used in HighResMIP is EC-Earth3.2.P. Compared to version 2.3, EC-Earth3.2.P includes updated versions of its atmospheric and oceanic model components, as well as a higher horizontal and vertical resolution in the atmosphere.

The atmospheric component of EC-Earth is the Integrated Forecast System (IFS) of the European Centre for Medium Range Weather Forecasts (ECMWF). Based on cycle 36r4 of IFS, it is used at T255 and at T511 resolution for the standard and high resolution simulation in HighResMIP, respectively. It uses a reduced Gauss-grid with 91 vertical levels. The nominal resolution is about 100km x 100km in standard resolution and 50 x 50 km in high resolution.

The ocean component is the Nucleus for European Modelling of the Ocean (NEMO, (Madec, 2008)). It uses a tri-polar grid with poles over northern North America, Siberia and Antarctica with a resolution of about 1 degree (the so-called ORCA1-configuration) and 75 vertical levels (compared to 42 levels in the CMIP5 model version) in the standard resolution. In high resolution, the ORCA025 configuration is used with a resolution of about 0.25 degree.

The ocean model version is based on NEMO version 3.6 and includes the Louvain la Neuve sea-ice model version 3 (LIM3, (Vancoppenolle et al., 2012)), which is a dynamic-thermodynamic sea-ice model with five ice thickness categories.

The atmosphere and ocean/sea ice parts are coupled through the OASIS (Ocean, Atmosphere, Sea Ice, Soil) coupler.

The high-resolution configurations (T511 atmosphere and ORCA025 ocean, coupled or stand-alone) have been newly developed for EC-Earth 3. The high-resolution NEMO configuration is based on a set-up developed by the ShaCoNEMO collaboration and adapted to the specific atmosphere coupling used in EC-Earth. Particularly, the remapping of runoff from the atmospheric grid points to runoff areas on the ocean grid has been re-implemented to be independent of the grid resolution. This is done by introducing an auxiliary model component and relying on the interpolation routines provided by the OASIS coupler. In a similar manner, forcing data for the atmosphere is passed through a separate model component, which allows use of the same forcing data set for different EC-Earth configurations.

A full description of EC-Earth3.2.P and its ability to simulate the climate can be found in Haarsma (2018).

1.2 HadGEM3

HadGEM3-GC3.1 is described in Williams et al. (2018). The atmospheric only simulations used in this paper utilizes the Easy Aerosol scheme (Voigt et al., 2014) and the component configurations Global Atmosphere 7.1 (GA7.1), and JULES Global Land 7.1 (GL7.1) described in Walters et al. (2017). GA7.1 dynamical core ENDGame uses a semi-implicit semi-Lagrangian formulation to solve the non-hydrostatic, fully-compressible deep-atmosphere equations of motion (Wood et al., 2014). The microphysics used is based on Wilson and Ballard (1999), with extensive modifications described in more detail in Walters et al. (2017). The parametrisation used is the prognostic cloud fraction and prognostic condensate (PC2) scheme (Wilson et al., 2008a;Wilson et al., 2008b) along with the cloud erosion parametrisation described by Morcrette (2012) and critical relative humidity parametrisation described in Van Weverberg et al. (2016). The model uses 85 vertical levels with 50 levels below 18 km and 35 levels above this, and a fixed model lid 85 km above sea level. Three different horizontal resolutions of the regular lat-lon grid are used in this study: N96, N216 and N512, which correspond respectively to a grid cell size of 135km, 60km and 25km at 50ºN, and are referred to as LM, MM and HM in the rest of the paper. The UM uses a mass flux convection scheme based on Gregory and Rowntree (1990) with various extensions to include down-draughts (Gregory and Allen, 1991) and convective momentum transport (CMT).

1.3 CNRM-CM6

The atmospheric only simulations analysed in this study are based on the atmosphere-land component of CNRM-CM6 which consists in the atmospheric model ARPEGE-Climat version 6.3, fully described in (Roehrig, 2018), and the SURFEX v8 land surface scheme(Decharme, 2018). The ARPEGE-Climat dynamical core is derived from IFS cycle 37t1. The model is operated with a T127 and a T359 truncation, the associated horizontal resolution being 120 km and 50 km for the LR and HR versions respectively. In both versions there are 91 vertical levels in the atmosphere. Compared to CNRM-CM5, the atmospheric physics has been largely revisited. In particular, convection scheme, microphysics scheme and turbulent scheme have been updated. The convection scheme (Guérémy, 2011;Piriou et al., 2007) provides a consistent, continuous, and prognostic treatment of convection from dry thermals to deep precipitating events. The microphysics scheme is derived from Lopez (2002) and takes into account autoconversion, sedimendation, ice-melting, precipitation evaporation and collection. The turbulence scheme represents the TKE with a 1.5-order scheme prognostic equation according to Cuxart et al. (2000). Surface drag over oceans is capped in CNRM-CM6 (see Soloviev et al. (2014) for general discussion). The calculations of exchange coefficients over ocean are based on an updated version of the Exchange Coefficients from Unified Multi-campaigns Estimates (Belamari, 2005) scheme.

1.4 NICAM

NICAM (Satoh et al., 2008;Satoh et al., 2014;Tomita and Satoh, 2004) is a non-hydrostatic atmospheric model with the icosahedral grid system. Here, climate simulation output from 14 km mesh NICAM(Kodama et al., 2015) is used for an analysis. Horizontal resolution is approximately 14 km, and 38 vertical levels are configured up to around 40 km. Instead of using convection and large-scale condensation schemes, a single moment bulk cloud microphysics scheme (Tomita, 2008) is used, in which rain, snow, and graupel as well as water vapor, cloud water, and cloud ice are treated as prognostic variables. SST is not fixed but nudged toward its monthly-mean historical distributions (Kodama et al., 2015).

1.5 ICON

The experiment using the ICOsahedral Non-hydrostatic (ICON) atmospheric model applied here uses a non-hydrostatic dynamical core, like NICAM, on the icosahedral grid (Zängl et al., 2015). The 1-year run was conducted as part of a development towards kilometer-scale global simulations, and as such should be considered preliminary. The grid applied here has an equivalent grid-spacing of 10 km, and in the vertical 70 levels are applied with a top around 30 km. The atmospheric physics parameterizations are from the ICON-ESM (Giorgetta et al., 2018) typically applied at much lower resolutions, but here adapted to convective cloud-permitting scales. This includes turning off all moist convective parameterizations, shallow- mid- and deep convection, as well as disabling all sub-grid scale gravity wave parameterizations and changing certain tuning parameters. These changes were to set the critical relative humidity for cloud formation everywhere to unity, setting the sub-grid scale cloud inhomogeneity factors to unity, and setting the turbulence parameterization near-neutral turbulent Prandtl number to 0.7.

1.6 UM-CASIM

The simulations presented here are described fully in McCoy et al. (2018) – the following description is adapted in brief below. Simulations were performed in the MetOffice Unified Model (UM) vn10.3 based on GA6 (Walters et al., 2017) in a convection-permitting setting in aquaplanet mode (no continents or sea ice). The model was run at 0.088°x0.059° and neither convection parametrization nor cloud scheme were used. Simulations lasted for 15 days and were run with 70 vertical levels. The Cloud-AeroSol Interacting Microphysics (CASIM) two-moment microphysics scheme (Hill et al., 2015;Shipway and Hill, 2012;Grosvenor et al., 2017;Miltenberger et al., 2018) was used and is described in Shipway and Hill (2012). The warm rain processes in CASIM is compared to other microphysics schemes in Hill et al. (2015). The rain autoconversion and accretion rates parameterization used in CASIM are described in Khairoutdinov and Kogan (2000). Because these simulations are run in GA6 with CASIM microphysics they should not be directly compared to the HadGEM3 simulations in PRIMAVERA described above.

Sea surface temperature (SST) was held fixed in the simulations and the atmosphere was allowed to spin up for a week at low resolution and then for another week at high resolution. The SST profile used in the aquaplanet was derived from a 20-year climatology run from the UM in standard climate model configuration. The January SST from this run was reflected latitudinally to create two zonal-mean profiles of SST (the original and a reversed zonal-mean). The original and reflected SST were averaged together to create a symmetric SST.

Aerosol concentration is constant in the simulations. The aerosol profile was 100 cm^{-3} in the accumulation mode at the surface up until 5km and then exponentially decreased after 5km with an e-folding of 1 km. Aerosol-cloud interactions were parameterized using a simple Twomey-type parameterization of cloud droplet number concentration (CDNC) (Rogers and Yau, 1989) $CDNC = 0.5N_{acc}w^{0.25}$ with N_{acc} being accumulation mode aerosol number concentration and w being updraft velocity limited such that at w=16m/s CDNC= N_{acc}. The aerosol forcing in these simulations is highly idealized and is not intended to represent any sort of variation in aerosol properties in the same way as Easy Aerosol. The vertical velocity was set to have a minimum value of 0.1m/s. Ice number was controlled using a simple temperature-dependent relationship (Cooper, 1986). Because only two weeks of simulations were available for the UM-CASIM runs contours of SLP (as opposed to anomalies in SLP relative to the monthly-mean) were used to identify candidate cyclone centers as described in McCoy et al. (2018).

Figures

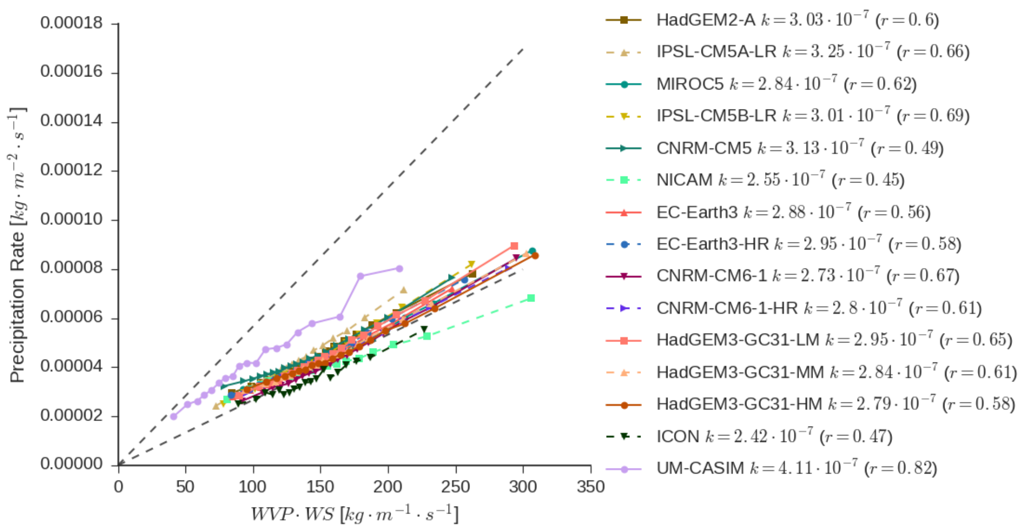

Fig. S 1 Cyclone-mean precipitation rate versus WCB moisture flux for the global models examined in this study. The *k* parameter (Field et al., 2011) for each model is noted in the legend along with the correlation between WCB moisture flux and cyclone-mean precipitation rate. The *k* parameter is calculated as the slope of the relationship between the product of WVP and WS_{10m} and the precipitation rate. Dashed lines show the observational bounds on *k* (Field et al., 2011;Naud et al., 2018). For ease of visualization the precipitation rates for each GCM are shown averaged into 19 quantiles of WVP_{CM}*WS_{10mCM}.

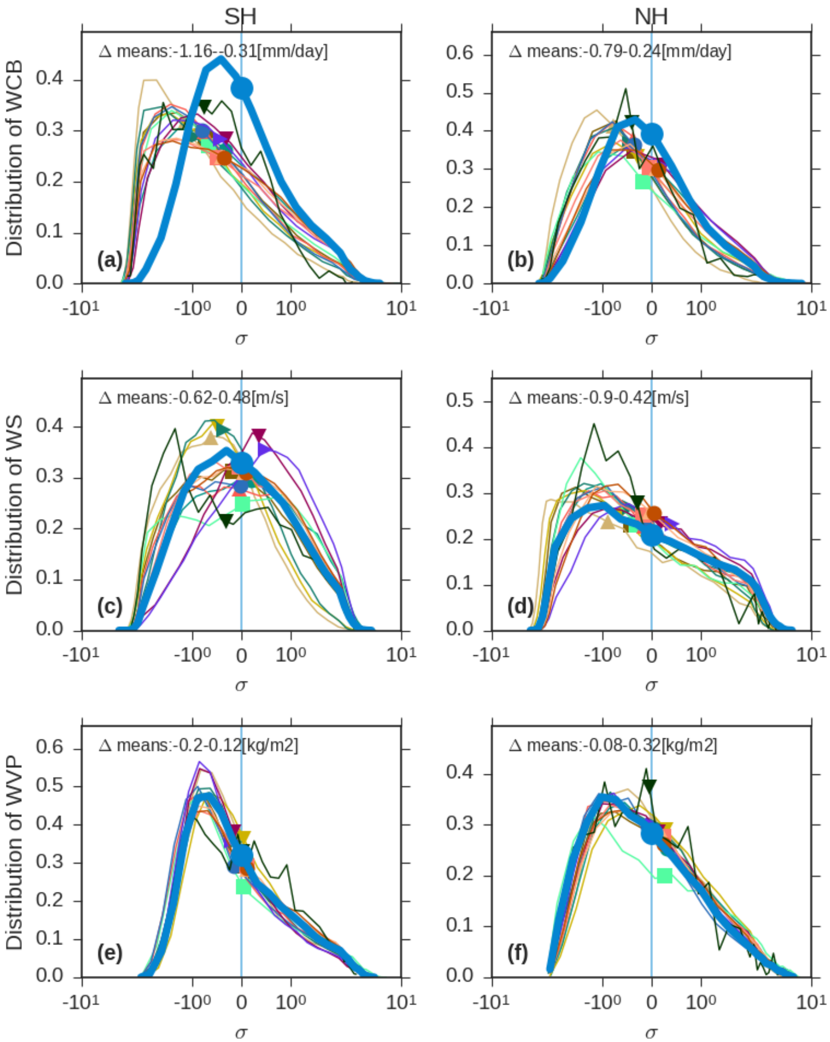

Fig. S 2 Normalized distributions of WCB moisture flux (a,b), 10-meter wind speed(c,d), and WVP(e,f) in extratropical cyclones. SH cyclones are shown in the left column and NH cyclones are shown in the right column. Distributions are normalized by subtracting the observed mean and dividing by the observed standard deviation. Means for each GCM and for the observations are shown using markers (as in Fig. 1). The range of the difference between the observed mean and the means of individual GCMs is noted in absolute units for each hemisphere and variable.

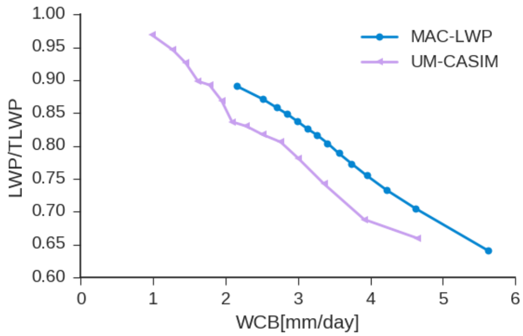

Fig. S 3 Cyclone-mean LWP (cloud) over TLWP (cloud+rain) calculated from the MAC-LWP observations and simulated by the UM-CASIM model as a function of WCB moisture flux. Observations and models are averaged into 14 equal quantiles of WCB moisture flux for visual clarity.

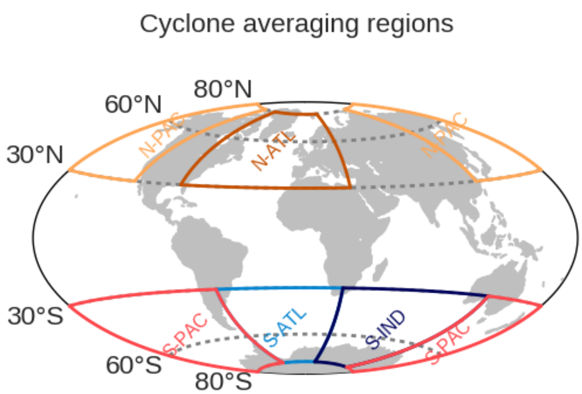

Fig. S 4 Averaging regions considered in this study. Labels refer to the North Pacific (N-PAC), North Atlantic (N-ATL), South Pacific (S-PAC), South Atlantic (S-ATL), and South Indian (S-IND) oceans.

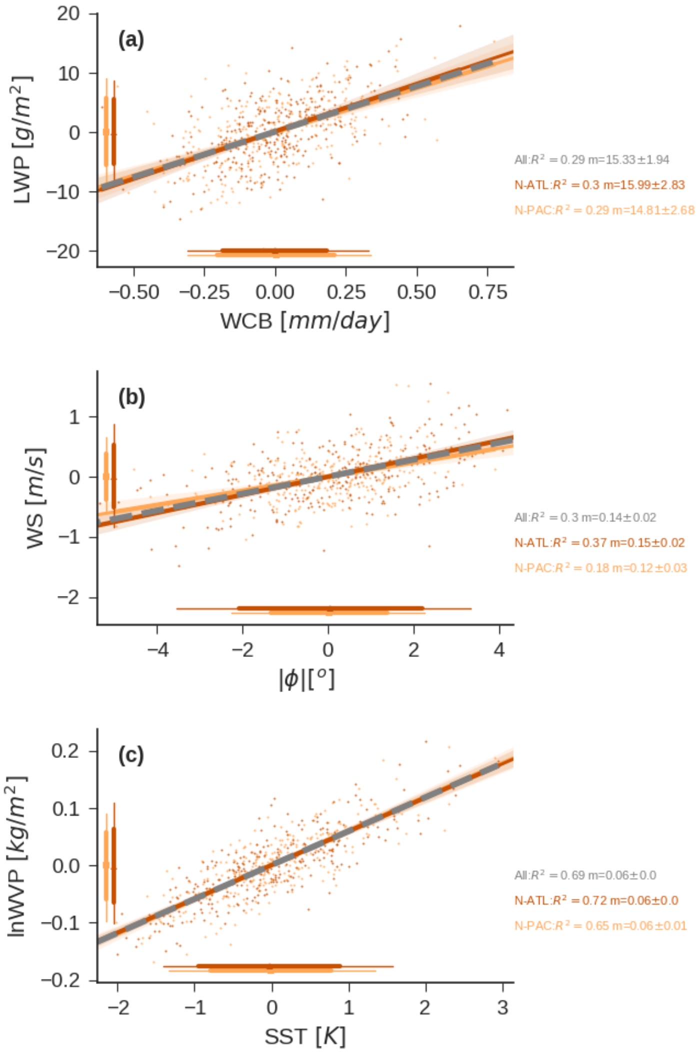

Fig. S 5 As in Fig. 2, but showing the NH.

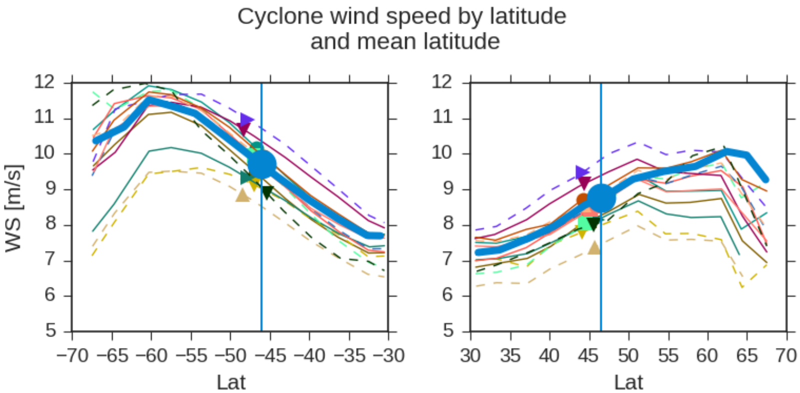

Fig. S 6 Cyclone-mean wind speed by latitude in observations (thick blue line) and models (as in Fig. 1). Markers denote mean cyclone location. Note that contributions from each month are weighted equally in the average.

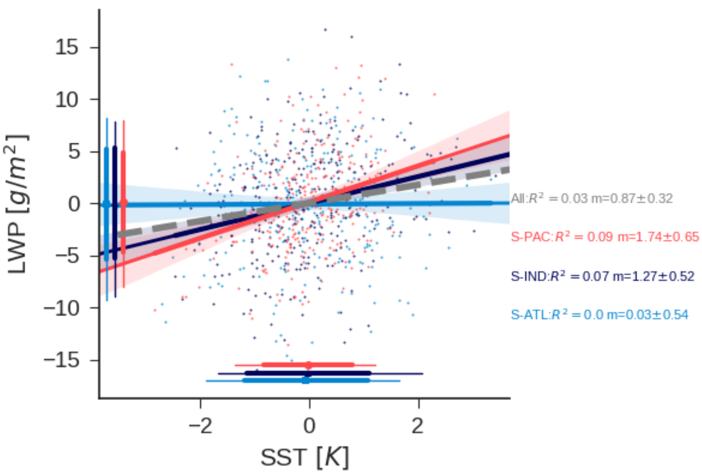

Fig. S 7 As in Fig. 2, but showing the relation between SST_{RM} and LWP_{RM}.

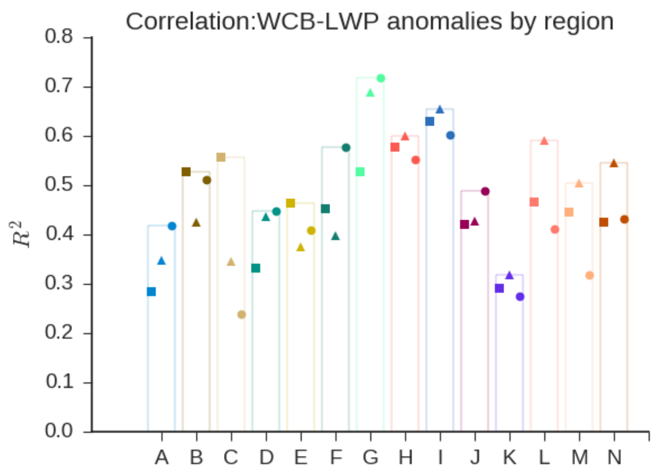

Fig. S 8 As in Fig. 3, but showing the R^2 between WCB moisture flux and LWP_{RM} monthly-mean anomalies for each basin in the models and observations.

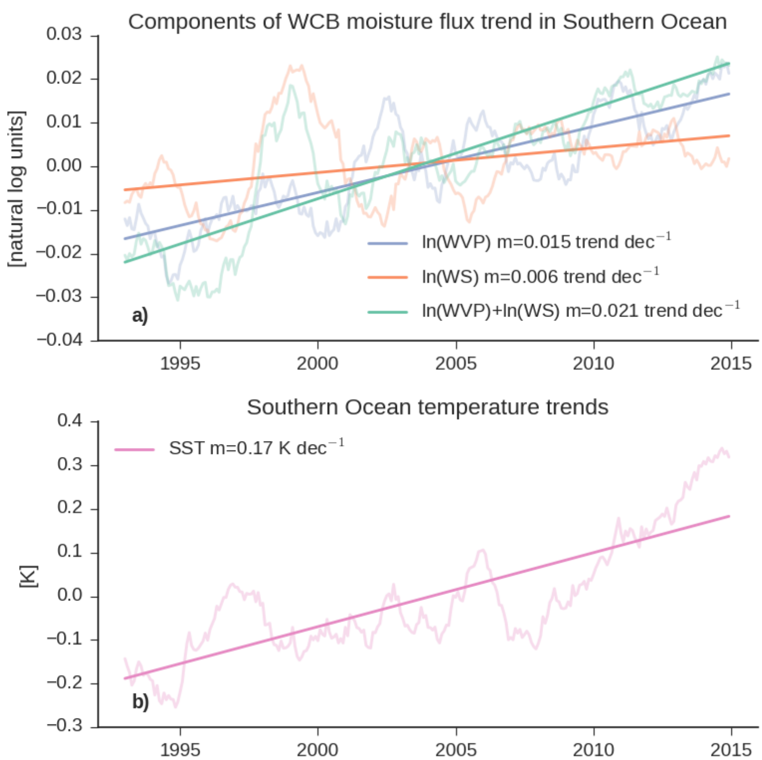

Fig. S 9 Trends in various cyclone-mean quantities for cyclones centered between 44.5°S and 59.5°S. (a) Trends in the natural log of cyclone-mean wind speed, WVP, and their sum. Note that $ln(WCB) = ln(k) + ln(WS_{10m}) + ln(WVP)$. The trend in units of

the natural log of each quantity per decade is given in the legend. Wind speed is in m/s, WVP is in kg/m². (b) the trend in SST within cyclones.

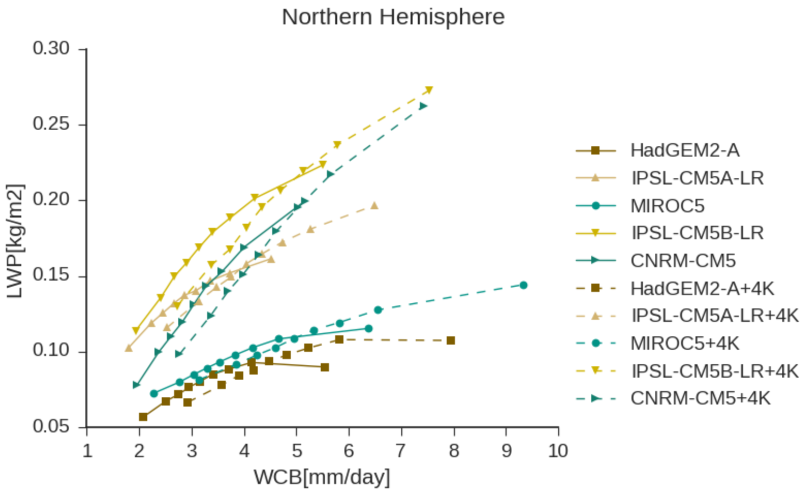

Fig. S 10 As in Fig. 6, but showing the NH.

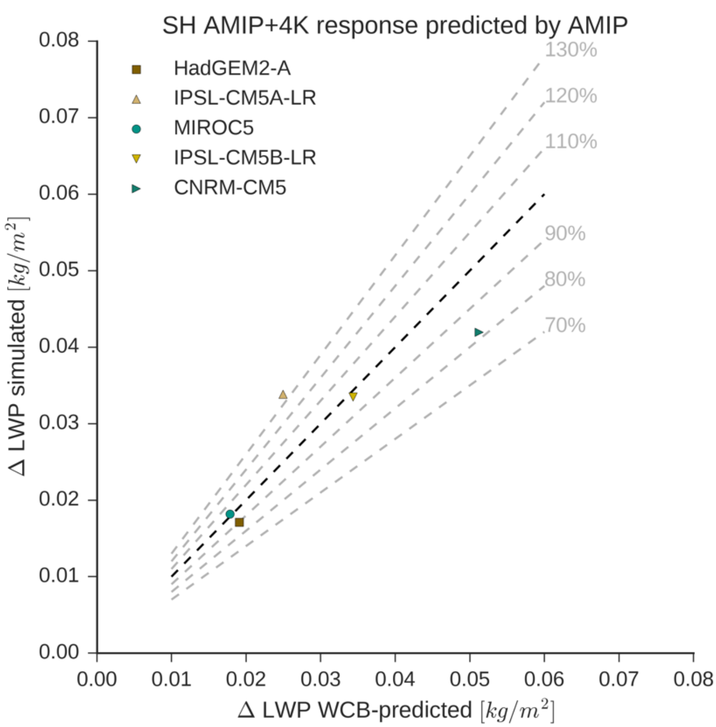

Fig. S 11 The difference in cyclone LWP in the SH between AMIP and AMIP+4K simulations versus the difference in SH cyclone LWP inferred from changes in WCB moisture flux and the relationship between WCB moisture flux and LWP_{CM} in the current climate. The one to one line is shown as a dark dashed line.

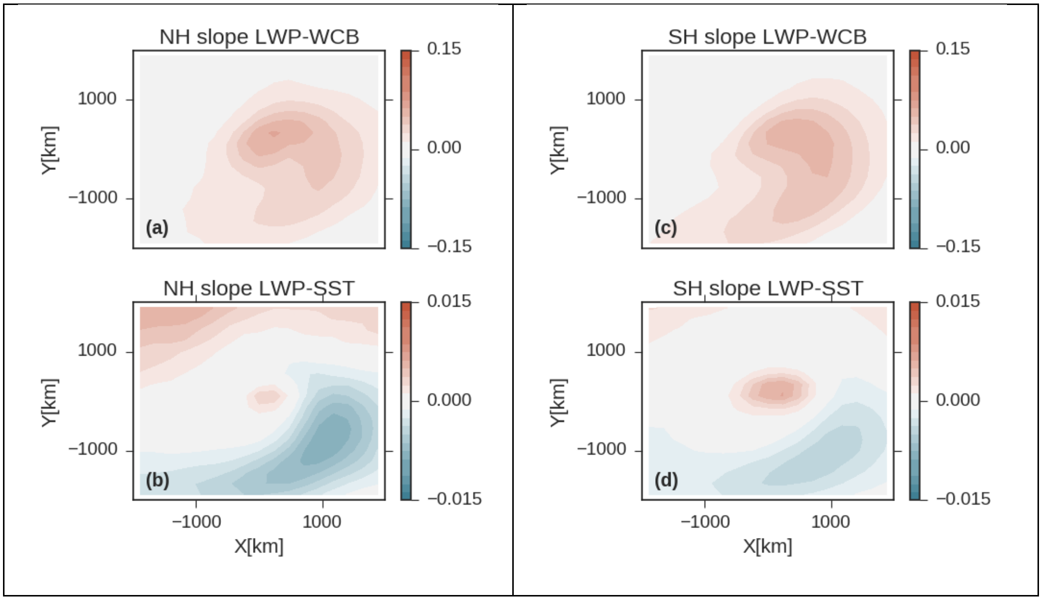

Fig. S 12 The multiple linear regression coefficients (Eq. 6) relating observations of LWP_{ij} to SST_{ij} and WCB moisture flux in the NH (a and b) and SH (c and d). Multiple linear regression is used to partition LWP_{ij} into contributions from SST_{ij} and WCB moisture flux. (a) and (c) show the slope of the linear regression between the WCB moisture flux into the cyclone and LWP_{ij} within the composite (units are kg mm day^{-1}m^{-2}). (b) and (d) show the regression coefficient relating SST_{ij} and LWP_{ij} (kg m^{-2}K^{-1}). Note that SH cyclones have been flipped vertically so that the top of the plot is to the pole to facilitate comparison to NH cyclones.

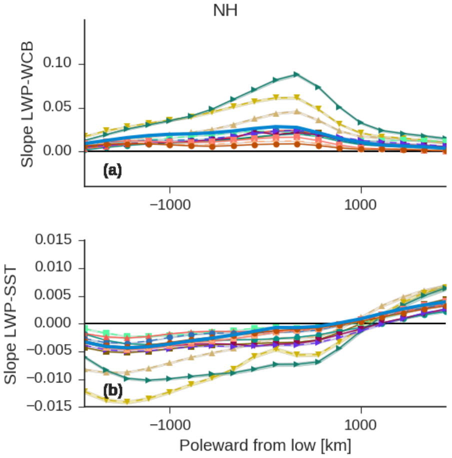

Fig. S 13 As in Fig. 9, but showing the NH.

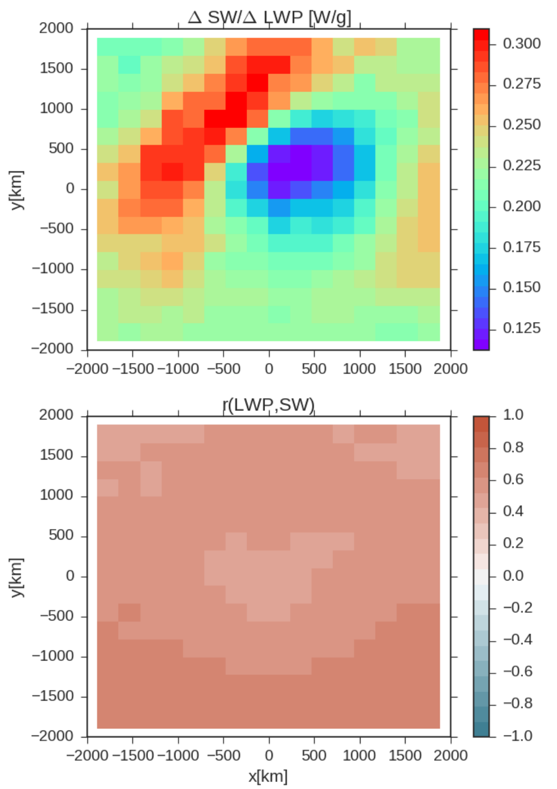

Fig. S 14 The regression coefficient relating changes in reflected shortwave radiation (SW_{ij}) to perturbations in LWP_{ij} across the cyclone composite (top). The correlation between variability in LWP_{ij} and SW_{ij} (bottom).

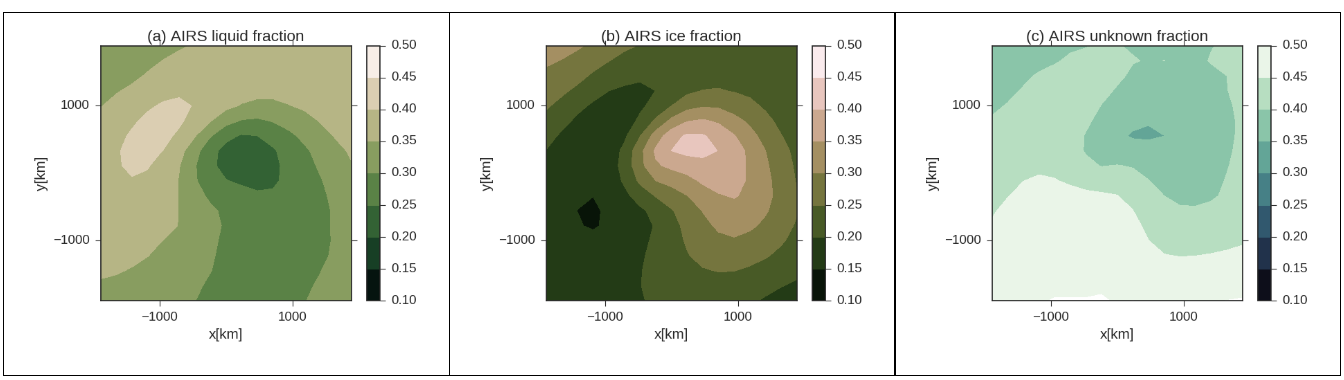

Fig. S 15 Fraction of liquid (a), ice (b), and unknown (c) cloud top phase from AIRS. Fractions are averages over the period 2003-2015 and are for both hemispheres.

References

Belamari, S.: Report on uncertainty estimates of an optimal bulk formulation for surface turbulent fluxes, Marine EnviRonment and Security for the European Area–Integrated Project (MERSEA IP), Deliverable D, 4, 2005.

Cooper, W. A.: Ice initiation in natural clouds, in: Precipitation Enhancement—A Scientific Challenge, Springer, 29-32, 1986.

Cuxart, J., Bougeault, P., and Redelsperger, J. L.: A turbulence scheme allowing for mesoscale and large-eddy simulations, Quarterly Journal of the Royal Meteorological Society, 126, 1-30, 2000.

Decharme, B.: In Preperation, 2018.

Field, P. R., Bodas-Salcedo, A., and Brooks, M. E.: Using model analysis and satellite data to assess cloud and precipitation in midlatitude cyclones, Quarterly Journal of the Royal Meteorological Society, 137, 1501-1515, 10.1002/qj.858, 2011.

Giorgetta, M. A., Brokopf, R., Crueger, T., Esch, M., Fiedler, S., Helmert, J., Hohenegger, C., Kornblueh, L., Köhler, M., and Manzini, E.: ICON-A, the atmosphere component of the ICON Earth System Model. Part I: Model Description, J. Adv. Model. Earth Syst., 2018.

Gregory, D., and Rowntree, P.: A mass flux convection scheme with representation of cloud ensemble characteristics and stability-dependent closure, Monthly Weather Review, 118, 1483-1506, 1990.

Gregory, D., and Allen, S.: The effect of convective scale downdrafts on NWP and climate simulations, Ninth Conference on Numerical Weather prediction, 1991, 122-123.

Grosvenor, D. P., Field, P. R., Hill, A. A., and Shipway, B. J.: The relative importance of macrophysical and cloud albedo changes for aerosol-induced radiative effects in closed-cell stratocumulus: insight from the modelling of a case study, Atmos. Chem. Phys., 17, 5155-5183, 10.5194/acp-17-5155-2017, 2017.

Guérémy, J.: A continuous buoyancy based convection scheme: one-and three-dimensional validation, Tellus A: Dynamic Meteorology and Oceanography, 63, 687-706, 2011.

Haarsma, R.: EC-Earth3.2.P - The PRIMAVERA version. , In Preperation
, 2018.

Hazeleger, W., Wang, X., Severijns, C., Ştefănescu, S., Bintanja, R., Sterl, A., Wyser, K., Semmler, T., Yang, S., and Van den Hurk, B.: EC-Earth V2. 2: description and validation of a new seamless earth system prediction model, Climate dynamics, 39, 2611-2629, 2012.

Hill, A. A., Shipway, B. J., and Boutle, I. A.: How sensitive are aerosol-precipitation interactions to the warm rain representation?, Journal of Advances in Modeling Earth Systems, 7, 987-1004, 10.1002/2014MS000422, 2015.

Khairoutdinov, M., and Kogan, Y.: A new cloud physics parameterization in a large-eddy simulation model of marine stratocumulus, Monthly weather review, 128, 229-243, 2000.

Kodama, C., Yamada, Y., Noda, A. T., Kikuchi, K., Kajikawa, Y., Nasuno, T., Tomita, T., Yamaura, T., Takahashi, H. G., Hara, M., Kawatani, Y., Satoh, M., and Sugi, M.: A 20-Year Climatology of a NICAM AMIP-Type Simulation, Journal of the Meteorological Society of Japan. Ser. II, 93, 393-424, 10.2151/jmsj.2015-024, 2015.

Lopez, P.: Implementation and validation of a new prognostic large-scale cloud and precipitation scheme for climate and data-assimilation purposes, Quarterly Journal of the Royal Meteorological Society, 128, 229-257, 2002.

Madec, G.: NEMO ocean engine: Note du Pôle de modélisation de l'Institut Pierre-Simon Laplace No 27, in, Tech. rep, 2008.

McCoy, D. T., Field, P. R., Schmidt, A., Grosvenor, D. P., Bender, F. A. M., Shipway, B. J., Hill, A. A., Wilkinson, J. M., and Elsaesser, G. S.: Aerosol midlatitude cyclone indirect effects in observations and high-resolution simulations, Atmospheric Chemistry and Physics, 18, 5821-5846, 10.5194/acp-18-5821-2018, 2018.

Miltenberger, A. K., Field, P. R., Hill, A. A., Rosenberg, P., Shipway, B. J., Wilkinson, J. M., Scovell, R., and Blyth, A. M.: Aerosol–cloud interactions in mixed-phase convective clouds – Part 1: Aerosol perturbations, Atmos. Chem. Phys., 18, 3119-3145, 10.5194/acp-18-3119-2018, 2018.

Morcrette, C. J.: Improvements to a prognostic cloud scheme through changes to its cloud erosion parametrization, Atmospheric Science Letters, 13, 95-102, 2012.

Naud, C. M., Booth, J. F., Lebsock, M., and Grecu, M.: Observational Constraint for Precipitation in Extratropical Cyclones: Sensitivity to Data Sources, Journal of Applied Meteorology and Climatology, 57, 991-1009, 10.1175/jamc-d-17-0289.1, 2018.

Piriou, J.-M., Redelsperger, J.-L., Geleyn, J.-F., Lafore, J.-P., and Guichard, F.: An approach for convective parameterization with memory: Separating microphysics and transport in grid-scale equations, Journal of the Atmospheric Sciences, 64, 4127-4139, 2007.

Roehrig, R.: In Preperation, 2018.

Rogers, R., and Yau, M.: A short course of cloud physics. Pregamon, in, Oxford, 1989.

Satoh, M., Matsuno, T., Tomita, H., Miura, H., Nasuno, T., and Iga, S.-i.: Nonhydrostatic icosahedral atmospheric model (NICAM) for global cloud resolving simulations, Journal of Computational Physics, 227, 3486-3514, 2008.

Satoh, M., Tomita, H., Yashiro, H., Miura, H., Kodama, C., Seiki, T., Noda, A. T., Yamada, Y., Goto, D., and Sawada, M.: The non-hydrostatic icosahedral atmospheric model: Description and development, Progress in Earth and Planetary Science, 1, 18, 2014.

Shipway, B. J., and Hill, A. A.: Diagnosis of systematic differences between multiple parametrizations of warm rain microphysics using a kinematic framework, Quarterly Journal of the Royal Meteorological Society, 138, 2196-2211, 10.1002/qj.1913, 2012.

Soloviev, A. V., Lukas, R., Donelan, M. A., Haus, B. K., and Ginis, I.: The air-sea interface and surface stress under tropical cyclones, Scientific Reports, 4, 5306, 10.1038/srep05306
https://www.nature.com/articles/srep05306#supplementary-information, 2014.

Tomita, H., and Satoh, M.: A new dynamical framework of nonhydrostatic global model using the icosahedral grid, Fluid Dynamics Research, 34, 357-400, 2004.

Tomita, H.: New microphysical schemes with five and six categories by diagnostic generation of cloud ice, Journal of the Meteorological Society of Japan. Ser. II, 86, 121-142, 2008.

Van Weverberg, K., Boutle, I. A., Morcrette, C. J., and Newsom, R. K.: Towards retrieving critical relative humidity from ground-based remote-sensing observations, Quarterly Journal of the Royal Meteorological Society, 142, 2867-2881, 2016.

Vancoppenolle, M., Bouillon, S., Fichefet, T., Goosse, H., Lecomte, O., Morales Maqueda, M., and Madec, G.: The Louvain-la-Neuve sea ice model, Notes du pole de modélisation, Institut Pierre-Simon Laplace (IPSL), Paris, France, 2012.

Voigt, A., Stevens, B., Bony, S., and Boucher, O.: Easy Aerosol–a modeling framework to study robustness and sources of uncertainties in aerosol-induced changes of the large-scale atmospheric circulation, WCRP, in, 2014.

Walters, D., Boutle, I., Brooks, M., Melvin, T., Stratton, R., Vosper, S., Wells, H., Williams, K., Wood, N., Allen, T., Bushell, A., Copsey, D., Earnshaw, P., Edwards, J., Gross, M., Hardiman, S., Harris, C., Heming, J., Klingaman, N., Levine, R., Manners, J., Martin, G., Milton, S., Mittermaier, M., Morcrette, C., Riddick, T., Roberts, M., Sanchez, C., Selwood, P., Stirling, A., Smith, C., Suri, D., Tennant, W., Vidale, P. L., Wilkinson, J., Willett, M., Woolnough, S., and Xavier, P.: The Met Office Unified Model Global Atmosphere 6.0/6.1 and JULES Global Land 6.0/6.1 configurations, Geosci. Model Dev., 10, 1487-1520, 10.5194/gmd-10-1487-2017, 2017.

Williams, K., Copsey, D., Blockley, E., Bodas-Salcedo, A., Calvert, D., Comer, R., Davis, P., Graham, T., Hewitt, H., and Hill, R.: The Met Office global coupled model 3.0 and 3.1 (GC3. 0 and GC3. 1) configurations, J. Adv. Model. Earth Syst., 10, 357-380, 2018.

Wilson, D. R., and Ballard, S. P.: A microphysically based precipitation scheme for the UK Meteorological Office Unified Model, Quarterly Journal of the Royal Meteorological Society, 125, 1607-1636, 1999.

Wilson, D. R., Bushell, A., Kerr-Munslow, A. M., Price, J. D., Morcrette, C. J., and Bodas-Salcedo, A.: PC2: A prognostic cloud fraction and condensation scheme. II: Climate model simulations, Quarterly Journal of the Royal Meteorological Society, 134, 2109-2125, 2008a.

Wilson, D. R., Bushell, A. C., Kerr-Munslow, A. M., Price, J. D., and Morcrette, C. J.: PC2: A prognostic cloud fraction and condensation scheme. I: Scheme description, Quarterly Journal of the Royal Meteorological Society, 134, 2093-2107, 2008b.

Wood, N., Staniforth, A., White, A., Allen, T., Diamantakis, M., Gross, M., Melvin, T., Smith, C., Vosper, S., and Zerroukat, M.: An inherently mass-conserving semi-implicit semi-Lagrangian discretization of the deep-atmosphere global non-hydrostatic equations, Quarterly Journal of the Royal Meteorological Society, 140, 1505-1520, 2014.

Zängl, G., Reinert, D., Rípodas, P., and Baldauf, M.: The ICON (ICOsahedral Non-hydrostatic) modelling framework of DWD and MPI-M: Description of the non-hydrostatic dynamical core, Quarterly Journal of the Royal Meteorological Society, 141, 563-579, 2015.